Evaluation of PM Rotor Topologies for Impedance Matching of Small-Scale Passive DC-Connected Wind Generator Systems

C.J.J. Labuschagne, *Student Member, IEEE,* and M.J. Kamper, *Senior Member, IEEE*

***Abstract*—This paper forms part of a broader study that investigates the design of permanent magnet synchronous generators for small-scale passive dc-connected wind energy systems. Achieving satisfactory power matching between the wind generator and the wind turbine is often difficult with these systems and a method of impedance matching is necessary. In this paper, generators with different interior permanent magnet rotor topologies are compared with a surface-mounted permanent magnet rotor in terms of dc-grid impedance matching to obtain maximum turbine power point matching. The different wind generator topologies are optimised in a design process whereby internal impedance matching is reached as far as possible. It is shown that only the interior permanent magnet rotor topology generators satisfy the required internal impedance matching. The spoke-type interior permanent magnet generator is found to be superior.**

***Index Terms*—direct-drive, impedance matching, multi-objective optimisation, non-overlap winding, passive wind energy system, permanent magnet synchronous generator, small-scale wind turbine, wind generator**

I. Introduction

It is often within the interest of design engineers to alter a machine's design or topology for a specific application. In this paper, the application is for using permanent magnet synchronous generators (PMSG) in small-scale passive wind energy systems. The passive wind energy system is shown in Fig. 1. For small-scale wind turbines the PMSG is a pupular generator choice in industry [1] and the PMSG typically has a surface-mounted PM (S-PM) rotor topology.

The passive wind energy system in Fig. 1 is very attractive to industry because of its simplicity and low cost. The PMSG is directly connected to the dc grid or battery storage via a diode bridge rectifier. The system uses no control and no power electronic converters. Therefore, to ensure good power matching with the wind turbine, it is important that the PMSG's impedance Z_i in Fig. 1 matches correctly with the dc grid voltage. Also note that for the passive system it is important to account for the combined impedance of the brush-and slip-rings in the turbine nacelle and the transmission cable, Z_c, in Fig. 1.

Consider the example with the wind turbine power curves in Fig. 2: power curves B, C and D are examples of PMSGs directly connected in a passive wind energy system as in Fig. 1. It is desired that the PMSG for a passive system matches the maximum power of the wind turbine at the rated wind and turbine speed indicated by n_r. Power curve B is an example of where the internal impedance Z_i of the PMSG Fig. 1 is too small. Power curve C is an example of where the PMSG's internal impedance is too large. In the case of power curve D, the internal impedance of the PMSG matches with the load and the desired power matching with the wind turbine at the maximum power operating point is achieved.

The examples in Fig. 2 illustrate the importance of impedance matching in small-scale passive wind energy systems. Additionally, it is highlighted by [2] how important it is for small-scale wind energy systems to have good power matching at low wind speeds. This makes the PMSG design for impedance matching all the more challenging. In [3] and [4], PMSGs are designed for a small-scale passive wind energy system. However, the design approach does not guarantee good

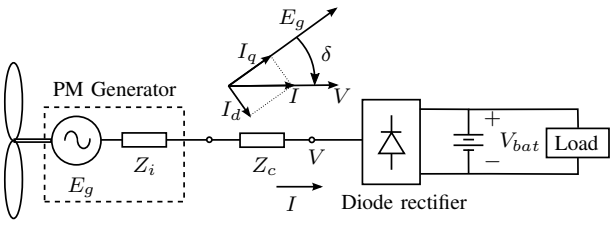

Fig. 1. Single-line diagram of PM wind generator connected to passive system with uncontrolled diode rectifier and battery storage.

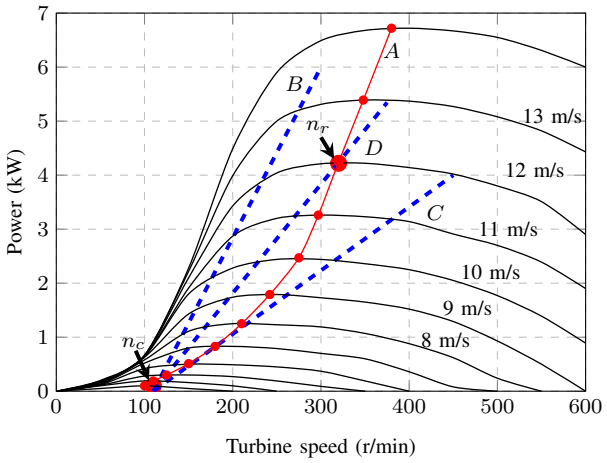

Fig. 2. Wind turbine power versus turbine speed curves with wind speed as a parameter, with examples of impedance matching with the wind generator.

This work was financially supported by the Centre for Renewable and Sustainable Energy Studies at Stellenbosch University, South Africa and by the Department of Science and Innovation (DSI) in South Africa.

C. J. J. Labuschagne and M. J. Kamper are with the Department of Electrical and Electronic Engineering, Stellenbosch University, Stellenbosch 7600, South Africa (e-mail: 17539455@sun.ac.za; kamper@sun.ac.za).

978-1-7281-9944-3/20/$31.00 ©2020 IEEE

power matching at low wind speeds. In [5], the PMSG is designed and then the wind turbine's parameters are adjusted for better power matching with the wind generator. Changing the wind turbine's parameters is not always desireable. In [6] and [7] the desired power matching with the wind turbine is achieved by adding an external inductance to the system. With this method of impedance matching the external inductance is added between the PMSG and the diode bridge rectifier in Fig. 1.

In [7] it was found that, when using non-overlap winding S-PM rotor PMSGs, external impedance matching is necessary for the passive system in Fig. 1. The necessary external inductance in [7] is quite large and, although the addition of the external inductance to the system is necessary and drastically improves the overall power matching, the extra component to the passive system is undesirable. It is therefore of interest to investigate alternative methods of "building" the necessary external inductance for maximum power matching into the PMSG.

In this paper different rotor topologies are considered in the PMSG design process as a method to "build" the external inductance into the PMSG. Altering the placement and the orientation of the PMs in the rotor changes the magnetic saliency of the machine and increases the synchronous inductance. It is therefore possible to have a larger internal synchronous impedance. In the paper the different PMSG topologies are designed for this application according to design specifications by making use of a multi-objective design optimisation strategy. With one of the objectives being to minimise the necessary external inductance, the design-optimisation results are used to compare the PMSG topologies and to determine whether altering the PM rotor is a feasible method to achieve built-in impedance matching.

II. System Specifications

The wind turbine power versus turbine speed curves for a 4.2 kW passive wind energy system are shown in Fig. 2. Also shown in Fig. 2 is the optimal available turbine power that can be extracted from the wind (power curve A). The passive wind energy system does not use any means of control, and therefore the PMSG needs to be carefully designed so that the generator's power curve matches well with the wind turbine's power curves. Thus, two operating points are specified for the PMSG i.e. (i) the cut-in speed operating point n_c at which the PMSG starts supplying power to the dc grid or battery storage and (ii) the rated speed operating point n_r where the maximum available power is generated. The cut-in and rated operating points are indicated on Fig. 2 and the system's specifications are summarised in Table I.

TABLE I
SUMMARY OF SPECIFIED OPERATING POINTS.

	n_c	n_r
Wind speed	3 m/s	12 m/s
Turbine speed	110 r/min	320 r/min
Generated power, P_g	0 kW	4.2 kW
Fixed battery/dc grid voltage	48 V	

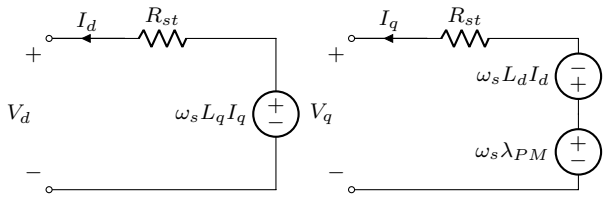

Fig. 3. Per-phase *dq*-equivalent circuit diagram of PMSG.

III. Mathematical Modelling

For a theoretical estimation of the necessary impedance, the PMSG is modelled in the *dq*-reference frame. From the *dq*-equivalent circuits in Fig. 3, the steady-state *dq*-equations are derived as

$$\begin{aligned} V_q &= -R_{st} I_q - \omega_s L_d I_d + \omega_s \lambda_{pm} \\ &= -R_{st} I_q - \omega_s L_d I_d + E_g \\ V_d &= -R_{st} I_d + \omega_s L_q I_q. \end{aligned} \tag{1}$$

In (1), R_{st} is the total resistance including the PMSG's stator resistance R_i, the resistance of the brush-slip rings and the resistance of the transmission cable R_c.

To explain the impedance matching of the system the analysis is simplified by assuming that R_{st} in Fig. 3 is zero. Considering the voltage equations in (1), we then have

$$\begin{aligned} V_q &= -\omega_s L_d I_d + E_g = -X_d I_d + E_g \\ V_d &= \omega_s L_q I_q = X_q I_q. \end{aligned} \tag{2}$$

With the wind generator system always operating at a fundamental power factor of unity due to the diode rectifier in the system of Fig. 1, the phasor diagram of Fig. 4(a) is obtained by using (2). The constrained terminal voltage V_b in Fig. 4 is the fixed fundamental per-phase voltage on the ac side of the diode rectifier. For the wind generator system, E_g in Fig. 4 is given by

$$E_g = aV_b \tag{3}$$

with

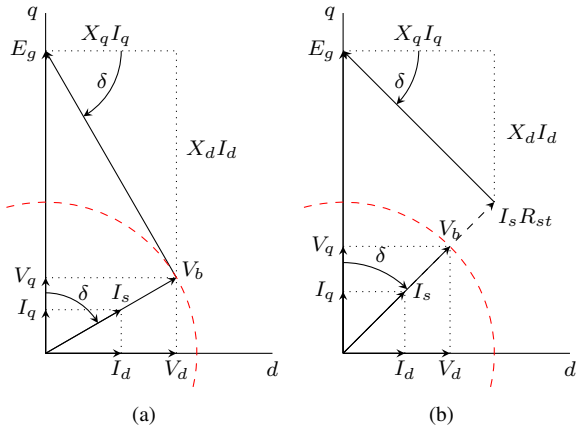

Fig. 4. Phasor diagrams of the passive wind generator system with (a) R_{st} excluded and (b) with R_{st} included.

TABLE II
PREDICTED *dq* VALUES AT RATED POWER.

$P = 1.0$ pu	$V_b = 1.0$ pu	$I_s = 1.0$ pu	$E_g = 2.91$ pu
$V_d = 0.94$ pu	$I_d = 0.94$ pu	$X_d = 2.73$ pu	
$V_q = 0.344$ pu	$I_q = 0.344$ pu	$X_q = 2.73$ pu	

$$a = \frac{n_r}{n_c}, \tag{4}$$

at rated power. In Fig. 4(a) this implies that

$$\cos(\delta) = \frac{V_b}{E_g} = \frac{1}{a} \Rightarrow \delta = \cos^{-1}\left(\frac{1}{a}\right). \tag{5}$$

Also from Fig. 4(a),

$$\tan(\delta) = \frac{V_d}{V_q} = \frac{I_d}{I_q} = \frac{X_d I_d}{X_q I_q} \Rightarrow \frac{X_d}{X_q} = 1.0. \tag{6}$$

For the wind turbine system $a = 2.91$ from Table I. Hence, from (5) we then have $\delta = 69.9°$. By substituting $\delta = 69.9°$ into (6) we have

$$\frac{I_d}{I_q} = \tan(69.9°) = 2.73 \tag{7}$$

With $V_b = I_s = 1.0$ pu, the per-unit values at rated power are calculated for the wind generator system and summarised in Table II.

The results in Table II are remarkable in terms of how high the per-unit reactance must be to have the correct impedance matching for maximum turbine power point matching. Bear in mind though, that the speed is also at 2.91 per unit. Taking this into account the per-unit reactance necessary at base speed is $X_d = X_q = 2.73/2.91 = 0.94$ per unit. The latter per-unit values, however, are still relatively high as S-PM machines with non-overlapping windings have per-unit reactance values that are typically between 0.2 to 0.4 per-unit. This simplified analysis thus shows that, on average, a per-unit reactance of three times higher than normal is required for correct impedance matching.

However, R_{st} in Fig. 3 cannot be ignored for the passive wind energy system's application in industry. The turbine-tower structure requires brushes on slip rings in the nacelle for the turbine's yawing, and the length of the transmission cable between the wind turbine and the dc grid/battery storage can typically be 50 m to 100 m. Furthermore, because of the constrained voltage V_b shown in Fig. 4 the system resembles a low-voltage, high-current system and therefore R_{st} would account for a significant voltage drop in the system. This is illustrated in the phasor diagram of the system in Fig. 4(b). Thus, the actual required per-unit reactance for correct impedance matching will be less than the predicted reactance in Table II, depending on the different impedance parameters of Z_c.

IV. PMSG TOPOLOGIES

In industry, low-speed direct-drive PMSGs are used in passive wind energy systems. An attractive PMSG slot-pole combination to use for the wind turbine in Fig. 2 is the 30-28 slot-pole combination with its double layer fractional-slot concentrated (non-overlap) winding. This slot-pole combination gives a very high fundamental winding factor of $k_{w7} \approx 0.951$ and machines with this slot-pole combination have been shown to have very low cogging torque [8]. The latter is very important for the starting of the small-scale wind turbine.

A. Stator Design

For the stator it is advantageous to have open slots with rectangular stator teeth. This allows for preformed coils to be used that are easy to manufacture and that have shorter end-winding lengths resulting in less copper losses. However, from the analysis in Section III the internal synchronous inductance of the PMSG must be increased. One way to achieve this is to use rectangular semi-closed stator slots to increase the stator leakage inductance. However, open slots that allow for preformed coils are preferred and is therefore chosen for all the PMSG designs as shown in Fig. 5(a).

B. Rotor Design

The rotor topologies considered for the PMSG design are also shown in Fig. 5. Fig. 5(b) shows the surface-mounted PM (S-PM) rotor topology, Fig. 5(c) the embedded PM (E-PM) rotor topology and Fig. 5(d) the interior spoke-type PM (ST-PM) rotor topology. Opting to use either surface (S-PM) or interior PM (E-PM and ST-PM) rotor topologies has certain trade-offs when it comes to manufacturing and machine performance.

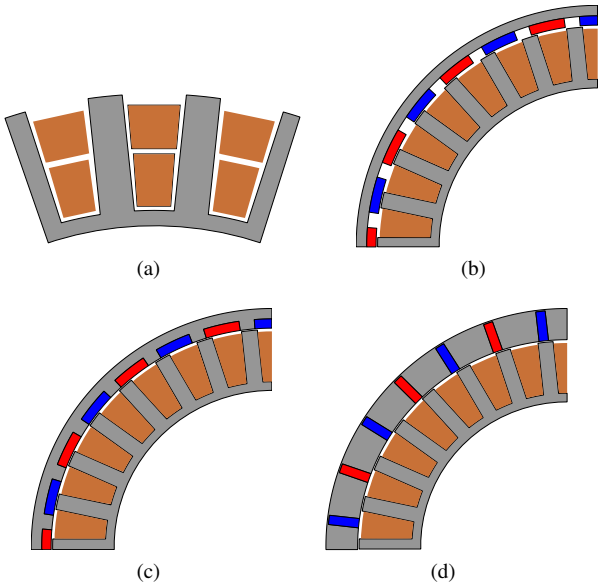

Fig. 5. Partial PMSG cross-sections illustrating (a) stator topology and different rotor topologies, (b) surface-mounted PM rotor (S-PM) (c), embedded PM rotor (E-PM) and (d) spoke-type interior PM rotor (ST-PM).

In the case of the S-PM rotors shown in Fig. 5(b), the manufacturing process is relatively simple and inexpensive. The S-PM rotor yoke generally uses less iron material which reduces the active mass of the PMSG. The latter reduction is important considering the need for a low top-tower wind turbine mass. The magnets on the rotor surface are exposed, however, and this could cause problems during assembly.

For interior PM rotor topologies, assembling the PMs during the manufacturing process has a low risk of damaging the PMs; the PMs can be slid into the rotor yoke lamination stack. Embedding the PMs in the rotor also has the additional advantage that the PMs are well protected against demagnetisation stator currents. In the case of the embedded rotor topologies shown in Fig. 5(c) and (d) it is obvious that the structure uses more iron material for the rotor yoke and would have a larger mass compared to the S-PM topology.

The potential higher top-tower mass would be a drawback for using embedded PMs in the rotor, even more so for the interior spoke PM rotors. Therefore, when comparing the PMSG designs it is important to take both the PM mass and the active mass of the PMSG into account. Designing the ST-PM rotor like the one in [9] could reduce the active mass; however, it could also compromise the structural integrity of the PMSG.

In [10] and [11], fractional-slot concentrated winding PMSGs with different rotor topologies are compared for direct-drive wind generators. It was found in [10] that machines with interior PM rotors can have higher pull-out torque and lower copper losses than surface PM machines with the same slot-pole combinations. The lower copper losses are important, especially for efficiency, as the copper losses dominate the core losses in the case of small-scale direct-drive wind generators.

C. Comparison of Rotor Topologies

As a result of using interior PM rotors, there is a significant increase in stator magnetisation flux compared to that of an S-PM rotor. It also results in a larger difference between the direct-axis and quadrature-axis inductances of the machine (also referred to as the magnetic saliency). Typical machine saliency properties for the different rotor topologies in Fig. 5 are summarised in Table III.

With the increase in stator magnetisation flux, the E-PM and ST-PM rotor machines have larger internal synchronous reactances than the S-PM rotor machine. These larger internal synchronous reactances of the interior PM rotor topologies might be sufficient in not requiring an additional external inductance for the PMSG's power matching with the wind turbine. Hence, it could be advantageous in this regard to opt

TABLE III
TYPICAL SALIENCY PROPERTIES OF THE DIFFERENT PMSG TOPOLOGIES IN FIG 5.

PMSG topology	Saliency
S-PM	$L_q \approx L_d$
IPM-E	$L_q > L_d$
IPM-ST	$L_q > L_d$

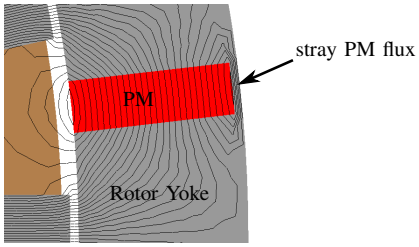

Fig. 6. Enlarged section of the IPM-ST rotor topology illustrating the PM flux paths and leakage flux.

to rather use the E-PM or ST-PM rotor topologies for small-scale passive wind energy systems instead of the S-PM rotor topology.

It should be noted that for the structural integrity of the ST-PM rotor the yoke needs support on at least one side of the interior embedded PM. Considering the illustration in Fig. 6, it is shown that the enclosed iron support section on the rotor yoke adds an additional path for stray leakage flux from the PMs.

V. DESIGN AND OPTIMISATION

A. Design Optimisation Strategy

For a comparison of the different rotor PMSGs, the PMSGs need to be design-optimised according to the system specifications and the performance constraints. Furthermore, it is important for this application to minimise the PMSG's cost and overall mass. Therefore, a multi-objective design optimisation process is used. For the design optimisation algorithm the population based NSGA-II (non-gradient sorting genetic algorithm II) [12] is used. The NSGA-II creates a pareto-optimal front with the non-dominated solutions by searching for a diverse set of solutions that satisfy the specified constraints and converge near the true pareto-optimal set.

To ensure that the desired impedance matching is achieved for all the solutions in the design optimisation, the impedance matching method of [7] is used, whereby an external inductance (L_{ext}) is added to the system as shown in Fig. 7. By giving L_{ext} to the optimisation algorithm as an output parameter that needs to be minimised, the optimisation results will include a set of solutions that eliminate L_{ext} from the passive system, i.e. where the PMSG's internal impedance alone is sufficient for good power matching.

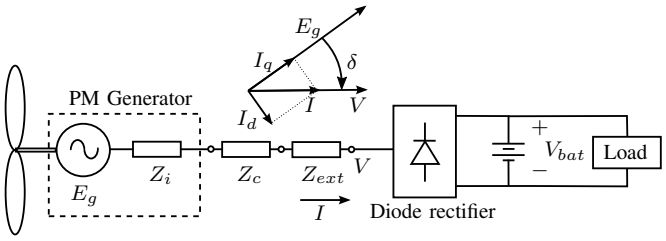

Fig. 7. Single-line diagram of PM wind generator with external inductance for impedance matching connected in passive wind turbine system.

The multi-objective function is given by

$$\min_{\mathbf{X}_n} \mathbf{F}(\mathbf{X}_n) = \min_{\mathbf{X}_n} \begin{bmatrix} M_{\text{active}}(\mathbf{X}_n) \\ M_{\text{PM}}(\mathbf{X}_n) \\ L_{ext}(\mathbf{X}_n) \end{bmatrix}, \tag{8}$$

subject to the performance constraints of the PMSG at the rated speed operating point n_r chosen as

$$\mathbf{U} = \begin{bmatrix} P_g \\ \eta \\ J \end{bmatrix} = \begin{bmatrix} 4.2 \text{ kW} \\ \geq 90 \text{ \%} \\ \leq 6 \text{ A/mm}^2 \end{bmatrix}. \tag{9}$$

In (8), M_{active} is the PMSG's active mass, M_{PM} is the PM mass of the PMSG and L_{ext} is the necessary external inductance for impedance matching. In (9), P_g is the generated power, η is the generator's efficiency and J is the RMS coil current density of the PMSG.

To solve the PMSG's performance and to calculate the necessary external inductance the 2D static FEA solution method of [7] is used. The method in [7] first calculates the number of coil turns in the PMSG for the desired cut-in speed voltage, then calculates the necessary external inductance to be added to the system for power matching and finally determines the PMSG's performance at the rated operating point.

B. Input Design Dimensions

In (8), $\mathbf{X}_n$ is the dimensional vector with the variables of each of the three machine topologies $n = 1, 2, 3$. The dimensions of the different machine topologies are defined in Fig. 8. For the S-PM and E-PM rotor topologies the dimensional vectors for the optimisation are given by $\mathbf{X}_1$ and $\mathbf{X}_2$ respectively, as

$$\mathbf{X}_1 = \mathbf{X}_2 = \begin{bmatrix} d_o & h_{y_r} & h_m & \sigma_m & h_s & w_t & h_{y_s} & l \end{bmatrix}^T, \tag{10}$$

where σ_m is the magnet-to-pole pitch ratio given by

$$\sigma_m = \frac{\theta_m}{\theta_p} \tag{11}$$

and l represents the axial length of the machine. For the ST-PM rotor topology the dimensional vector is given by $\mathbf{X}_3$ as

$$\mathbf{X}_3 = \begin{bmatrix} d_o & h_m & w_m & h_s & w_t & h_{y_s} & l \end{bmatrix}^T. \tag{12}$$

In this study the air-gap length is kept constant in the designs at $\delta_{air} = 1$ mm. For the ST-PM supporting structure h_{y_r} in Fig. 8(c) is taken as $h_{y_r} = 1$ mm.

VI. Optimisation Results

The design optimisation pareto front results of the M_{active} versus M_{PM} objectives are shown in Fig. 9 for the three rotor topologies. In Fig. 9 the third objective, to minimise L_{ext}, is indicated with a colour assignment. PMSG solutions in which the internal impedance of the PMSG is sufficient for power matching, i.e. $L_{ext} = 0$ mH, are plotted in blue and solutions in which $L_{ext} > 0$ mH are plotted in red.

For the S-PM rotor topology, the multi-objective optimisation results indicate that the pareto front in Fig. 9(a) struggled

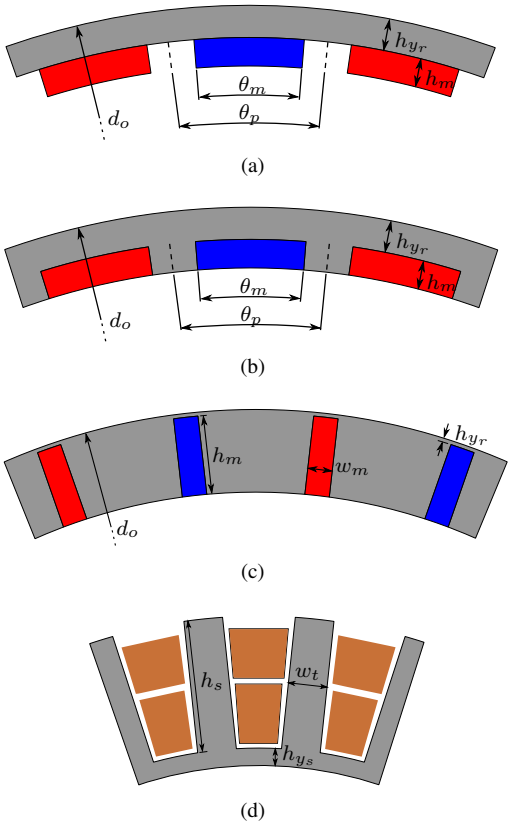

Fig. 8. Partial cross sections indicating the design dimensions for (a) the surface mounted PM rotor (S-PM), (b) the embedded PM rotor (E-PM), (c) the spoke-type interior PM rotor (ST-PM) and (d) open slot stator.

to converge as the internal impedance of none of the PMSG solutions was sufficient for power matching with the wind turbine. For all of the solutions it is necessary for an external inductance, L_{ext}, to be added to the system to achieve the desired power matching at the rated operating point.

For both the E-PM and ST-PM topologies in Fig. 9(b) and (c) respectively, it is shown that there are solutions for which the internal impedance of the PMSG alone is sufficient for power matching between the wind generator and the wind turbine. The performance results of an S-PM, E-PM and ST-PM rotor topology PMSG, chosen from the respective pareto fronts in Fig. 9, are compared in Table IV. These performance results of the PMSGs indicate that the constraints in (9) are met. Although the generated power, P_g, is slightly less than specified it is still deemed acceptable. Further, from Table IV it can be seen that the saliency ratios of the PMGSs are all very close to unity, as predicted by theory earlier. Note that the power angles δ in Table IV of between $54°$ and $62°$ are much smaller than the $69.9°$ as predicted earlier, but this is due to the relatively large resistance, R_{st}, as explained by the phasor diagram of Fig. 4(b).

The results in Fig. 9 and Table IV conclude that by simply changing the rotor topology it is possible to design a PMSG for the passive wind energy system that will match the wind turbine power without requiring any form of external impedance matching. To further illustrate this point the power curves of the E-PM and ST-PM rotor PMSGs in Table IV are plotted

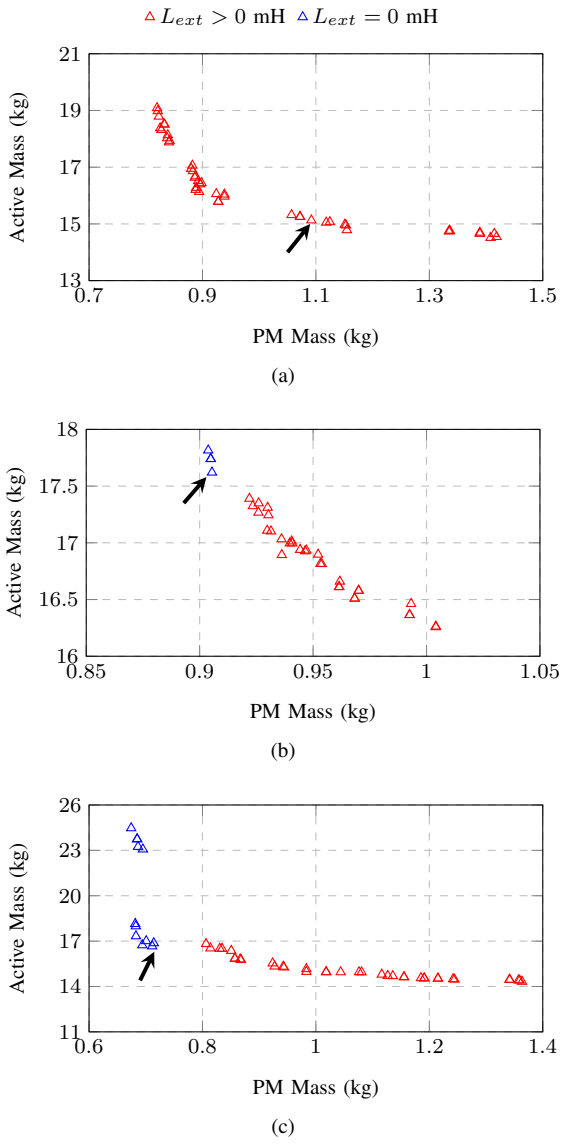

Fig. 9. PM mass versus active mass pareto front results with the L_{ext} objective as a colour gradient for (a) the surface-mounted PM rotor (S-PM), (b) the embedded PM rotor (E-PM) and (c) the spoke-type interior PM rotor (ST-PM) PMSGs.

against the wind turbine's power curves in Fig. 10. Both PMSGs start generating power at the specified cut-in speed and nearly match the available power at the specified rated operating point. Furthermore the generated power in general matches well with the available wind power for all turbine speeds, especially considering that no method of control is used.

In terms of the M_{active} and M_{PM} objectives in Fig. 9 and Table IV there are the following tradeoffs: For the S-PM topology M_{active} is less compared to the other two topologies. However, M_{PM} is much greater and the passive system still requires L_{ext} for impedance matching. The E-PM and ST-PM results indicate that there is very little tradeoff between the two interior rotor topologies. For the chosen pareto front solutions in Table IV, the ST-PM has a lower M_{active} and a lower M_{PM}. Considering the pareto fronts in Fig. 9(b) and (c), the ST-PM rotor topology solutions are consistently better than the E-PM rotor topology solutions in terms of M_{active} and M_{PM}.

TABLE IV
COMPARISON OF THE CHOSEN S-PM, E-PM AND ST-PM ROTOR TOPOLOGY PMSGS.

	S-PM	E-PM	ST-PM
M_{PM}, kg	1.09	0.904	0.71
M_{active}, kg	15.13	17.82	16.72
L_{ext}, mH	0.88	0.0	0.0
P_g, kW	4.17	4.06	4.12
η, %	90.0	90.0	90.0
J, A/mm^2	5.95	6.0	5.93
L_d, mH	1.60	2.83	2.51
L_q, mH	1.78	3.89	3.03
ξ	1.11	1.37	1.21
L_s, mH	2.14	3.76	3.22
X_s, pu	1.20	2.22	2.00
δ, °	54.4	61.9	57.3
d_o, mm	389	373	393
l, mm	41	53	42

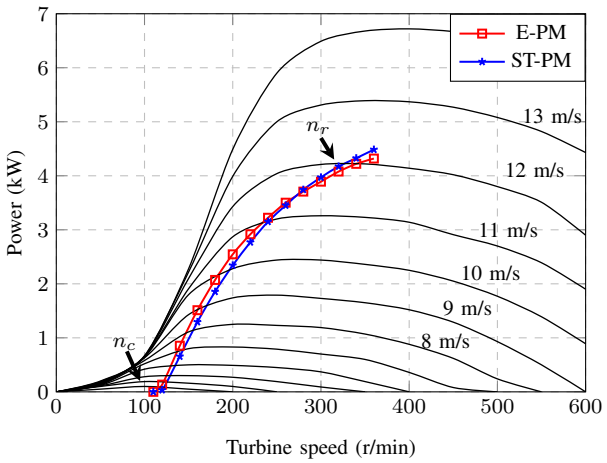

Fig. 10. Static FEA calculated power curves of the E-PM and ST-PM PMSGs from Table IV.

VII. CONCLUSIONS

In this paper PMSGs with different rotor topologies are considered for the wind generator design of a passive wind energy system. This is done to investigate whether the resulting higher internal impedance from using interior PM rotors is a sufficient method to achieve power matching with the wind turbine. The following main conclusions are drawn from the investigation:

- It was found that for both the E-PM and ST-PM rotor topologies the larger internal impedance of the PMSG, as a result of the additional stator magnetisation flux, is sufficient for the PMSG to achieve the desired power matching with the wind turbine in the generator design.

- In the case of the S-PM rotor it is shown that when using this topology PMSG in small-scale passive wind energy systems, external impedance matching is necessary for obtaining the desired power matching; hence, an external inductance needs to be added between the generator and the uncontrolled diode bridge rectifier.

- The optimal designs from the interior PM rotor topology's pareto fronts indicate that neither is excessively penalised in terms of the total active mass and PM mass. Besides the ability to achieve desirable power matching with only the generator's synchronous impedance, the overall performance is also satisfactory and within the set of design constraints. Therefore wind generators with interior PMs in the rotor are a very attractive alternative for generator design in passive wind energy systems, especially the ST-PM rotor topology.

REFERENCES

[1] Z. Alnasir and M. Kazerani, "An analytical literature review of stand-alone wind energy conversion systems from generator viewpoint," *Renewable and Sustainable Energy Reviews*, vol. 28, pp. 597–615, 2013.

[2] S. O. Ani, H. Polinder, and J. A. Ferreira, "Comparison of energy yield of small wind turbines in low wind speed areas," *IEEE Transactions on Sustainable Energy*, vol. 4, no. 1, pp. 42–49, Jan 2013.

[3] B. Sareni, A. Abdelli, X. Roboam, and D.-H. Tran, "Model simplification and optimization of a passive wind turbine generator," *Renewable Energy*, vol. 34, no. 12, pp. 2640–2650, 2009.

[4] D. Tran, B. Sareni, X. Roboam, and C. Espanet, "Integrated optimal design of a passive wind turbine system: An experimental validation," *IEEE Transactions on Sustainable Energy*, vol. 1, no. 1, pp. 48–56, April 2010.

[5] J. Aredjodoun, P. Chetangny, S. Houndedako, A. Vianou, D. Chamagne, and C. Espanet, "Optimal adaptation of the wind rotor to the permanent magnets synchronous generator of a small passive wind turbine," in *2019 IEEE PES/IAS PowerAfrica*. IEEE, 2019, pp. 164–169.

[6] F. G. Rossouw and M. J. Kamper, "Use of air-cored axial flux permanent magnet generator in direct battery charging wind energy systems," in *2007 7th International Conference on Power Electronics and Drive Systems*, Nov 2007, pp. 1102–1107.

[7] C. J. J. Labuschagne and M. J. Kamper, "Performance analysis of direct-drive PM synchronous wind generator for maximum power point direct battery charging," in *2018 XIII International Conference on Electrical Machines (ICEM)*, Sep. 2018, pp. 358–364.

[8] ——, "Design optimisation and comparison of fractional-slot overlap and non-overlap winding direct-drive PM wind generators for dc-connected applications," in *2019 IEEE Energy Conversion Congress and Exposition (ECCE)*, Sep. 2019, pp. 724–731.

[9] M. Chirca, C. Oprea, P.-D. Teodosescu, and S. Breban, "Optimal design of a radial flux spoke-type interior rotor permanent magnet generator for micro-wind turbine applications," in *2016 International Conference on Applied and Theoretical Electricity (ICATE)*. IEEE, 2016, pp. 1–5.

[10] P. Salminen, J. Pyrhonen, H. Jussila, and M. Niemela, "Concentrated wound permanent magnet machines with different rotor designs," in *2007 International Conference on Power Engineering, Energy and Electrical Drives*. IEEE, 2007, pp. 514–517.

[11] H. Chen, R. Qu, J. Li, and B. Zhao, "Comparison of interior and surface permanent magnet machines with fractional slot concentrated windings for direct-drive wind generators," in *2014 17th International Conference on Electrical Machines and Systems (ICEMS)*. IEEE, 2014, pp. 2612–2617.

[12] K. Deb, S. Agrawal, A. Pratap, and T. Meyarivan, "A fast elitist non-dominated sorting genetic algorithm for multi-objective optimization: NSGA-II," in *International conference on parallel problem solving from nature*. Springer, 2000, pp. 849–858.

VIII. BIOGRAPHIES

Casper J. J. Labuschagne received the B.Eng. degree in electrical and electronic engineering in 2016 from the Stellenbosch University, Stellenbosch, South Africa, where he is currently working towards the Ph.D. degree in electrical engineering.

Maarten J. Kamper (SM'08) received the M.Sc. (Eng.) and Ph.D. (Eng.) degrees from Stellenbosch University, Stellenbosch, South Africa, in 1987 and 1996, respectively. He has been a member of the Academic Staff at the Department of Electrical and Electronic Engineering at Stellenbosch University since 1989, where he is currently a Professor of electrical machines and drives. His research interests include computer-aided design and control of reluctance, permanent-magnet and induction machine drives. Prof. Kamper is a South African National Research Foundation-supported Scientist and a Registered Professional Engineer in South Africa.